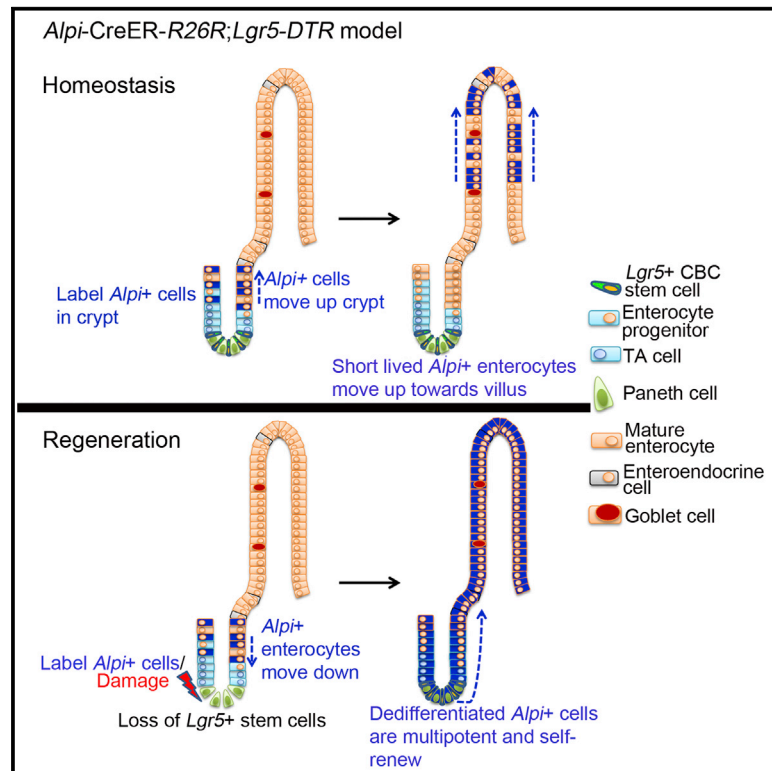


Cell Stem Cell

Replacement of Lost *Lgr5*-Positive Stem Cells through Plasticity of Their Enterocyte-Lineage Daughters

Graphical Abstract



Authors

Paul W. Tetteh, Onur Basak, Henner F. Farin, ..., Johan H. van Es, Alexander van Oudenaarden, Hans Clevers

Correspondence

h.clevers@hubrecht.eu

In Brief

In this article, Tetteh et al. show that enterocyte-lineage progenitors can become stem cells during intestinal regeneration. Additionally, these cells generate Paneth-like cells and turn on genes that promote recovery from injury. In sum, “stemness” in intestinal crypts is not “hard-wired;” many progenitors can regain stemness upon loss of the actual stem cells.

Highlights

- Enterocytes in intestinal crypts can dedifferentiate to replace lost *Lgr5*⁺ stem cells
- Dedifferentiating enterocytes generate proliferative stem cells and Paneth-like cells
- Enterocytes with *Apc/Kras* mutations do not form tumors in vivo
- “Stemness” in intestinal crypts is not “hard-wired”



Replacement of Lost *Lgr5*-Positive Stem Cells through Plasticity of Their Enterocyte-Lineage Daughters

Paul W. Tetteh,^{1,3} Onur Basak,¹ Henner F. Farin,^{1,4} Kay Wiebrands,¹ Kai Kretschmar,¹ Harry Begthel,¹ Maaïke van den Born,¹ Jeroen Korving,¹ Frederic de Sauvage,² Johan H. van Es,¹ Alexander van Oudenaarden,¹ and Hans Clevers^{1,*}

¹Hubrecht Institute, Royal Netherlands Academy of Arts and Sciences and University Medical Center, Utrecht, Uppsalalaan 8, 3584 CT Utrecht, the Netherlands

²Molecular Oncology Department, Genentech, South San Francisco, CA 94080, USA

³Present address: Laboratory of Immunobiology, Department of Medical Oncology, Dana-Farber Cancer Institute, Boston, MA 02215, USA

⁴Present address: Georg-Speyer-Haus, Institute for Tumor Biology and Experimental Therapy, Paul-Ehrlich-Strasse 42-44, 60596 Frankfurt, Germany

*Correspondence: h.clevers@hubrecht.eu

<http://dx.doi.org/10.1016/j.stem.2016.01.001>

SUMMARY

Intestinal crypts display robust regeneration upon injury. The relatively rare secretory precursors can replace lost stem cells, but it is unknown if the abundant enterocyte progenitors that express the Alkaline phosphatase intestinal (*Alpi*) gene also have this capacity. We created an *Alpi-IRES-CreERT2* (*Alpi^{CreER}*) knockin allele for lineage tracing. Marked clones consist entirely of enterocytes and are all lost from villus tips within days. Genetic fate-mapping of *Alpi*⁺ cells before or during targeted ablation of *Lgr5*-expressing stem cells generated numerous long-lived crypt-villus “ribbons,” indicative of dedifferentiation of enterocyte precursors into *Lgr5*⁺ stems. By single-cell analysis of dedifferentiating enterocytes, we observed the generation of Paneth-like cells and proliferative stem cells. We conclude that the highly proliferative, short-lived enterocyte precursors serve as a large reservoir of potential stem cells during crypt regeneration.

INTRODUCTION

In mammals, the intestinal epithelium is the fastest self-renewing tissue (Clevers, 2013). The rapid cellular turnover of the single-layered intestinal epithelium is powered by proliferation in the crypts of Lieberkühn to generate differentiated villus cells. Actively cycling crypt base-resident *Lgr5*⁺ stem cells (Barker et al., 2007) generate precursors of secretory cells and of enterocytes that divide while moving upward terminally differentiating into either goblet cells and enteroendocrine cells or into nutrient-absorbing enterocytes. The atypical Paneth cells belong to the secretory lineage, yet reside at crypt bottoms, are long-lived, and contribute to the stem cell niche (Sato et al., 2011).

Crypts display a remarkable regenerative capacity following DNA and cytotoxic damage (Withers, 1971) or, for instance, sur-

gical resection (Bernal et al., 2005). Although surviving stem cells play a critical role in this regenerative process (van der Flier et al., 2009a), it has been proposed that a quiescent stem cell population residing at the +4 position and expressing markers such as *Bmi1*, *mTert*, *Lrig1*, and *Hopx* (Sangiorgi and Capecchi, 2008; Takeda et al., 2011; Powell et al., 2012; Montgomery et al., 2011) function as reserve stem cells upon depletion of the actively cycling stem cell pool. As an alternative mechanism, intestinal regeneration may be driven by dedifferentiation of committed progeny. As implied by a recent study, radiation-sensitive cells occupying cell position 6 and above can replenish loss of *Lgr5*⁺ stem cells (Metcalfe et al., 2013). During homeostasis, secretory progenitors derived from *Lgr5*⁺ stem cells expressing *Dll1* generate short-lived clones composed of Paneth cells, goblet cells, enteroendocrine cells, and tuft cells. Lineage tracing followed by irradiation in *Dll1^{GFP-IRES-CreERT2}* mice indicated that *Dll1*⁺ cells dedifferentiated to stem cells in vivo to replenish lost stem cells, generating long-lived stem cell-driven crypt-villus ribbons (van Es et al., 2012).

Recently, an elegant study corroborated the involvement of secretory precursors in intestinal regeneration. It was observed that a quiescent label-retaining cell (LRC) population predominantly populates the +4 position and expresses *Lgr5* as well as the proposed markers of +4 cells such as *Bmi1*, *mTert*, *HopX*, and *Lrig1*. During homeostasis, these LRCs (which derive from *Lgr5*⁺ stem cells) serve as short-lived precursors of Paneth and enteroendocrine cells. However, upon loss of proliferative crypt cells induced by cytotoxic damage with doxorubicin, these LRCs dedifferentiate to *Lgr5*⁺ stem cells (Buczacki et al., 2013). It appears likely that these non-dividing secretory precursors represent the reserve stem cells located at the +4 position.

RESULTS

Enterocyte Marker *Alpi* Is Not Expressed in *Lgr5*⁺ CBC Stem Cells or *Dll1*⁺ Secretory Progenitors

We sought to establish if the most abundant and most proliferative cell type in the crypt, the enterocyte precursor, display plasticity upon stem cell loss. Previous gene expression datasets

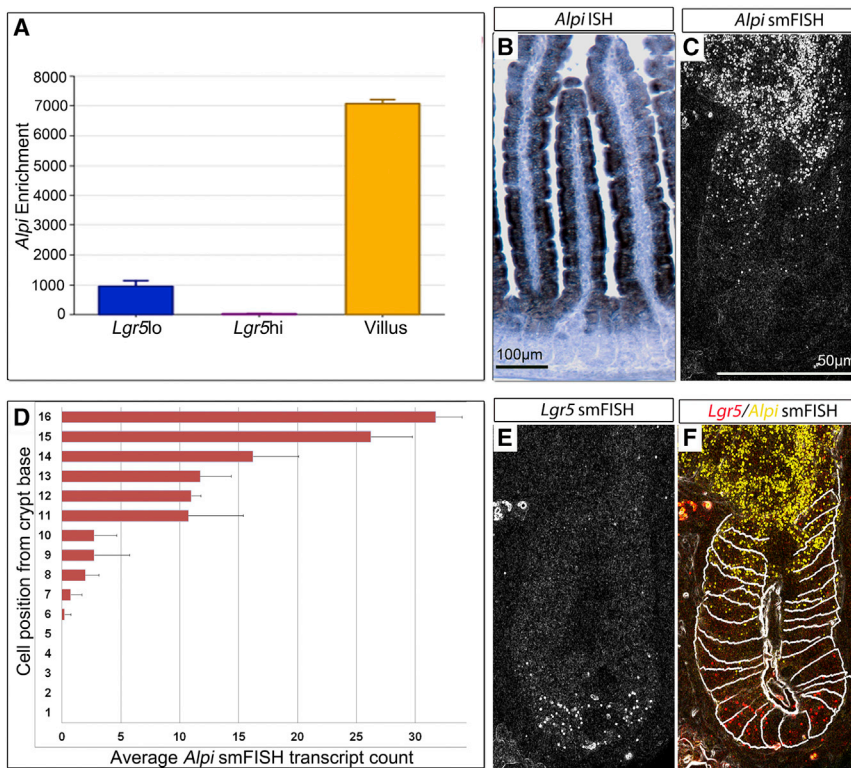


Figure 1. Expression of *Alpi* in Intestinal Crypts

(A) Microarray enrichment of *Alpi* in *Lgr5^{low}*, *Lgr5^{high}*, and villus fractions. *Alpi* is not expressed in *Lgr5^{high}* cells. Error bars represent \pm SEM.

(B) In situ hybridization (ISH) of *Alpi* in the intestinal crypt; *Alpi* is not expressed in lower crypt cells.

(C) Single-molecule FISH (smFISH) for *Alpi*. Dots represent *Alpi* mRNA transcripts localized in upper crypt cells.

(D) Quantification of crypt positions of *Alpi* transcripts, which can be detected from position +6 and progressively increasing to the top of the crypt.

(E) Single-molecule FISH for *Lgr5*.

(F) *Lgr5* transcripts (red dots) localize at the crypt bottom and do not overlap with *Alpi* transcripts (yellow dots).

See also Figure S1.

involving microarray analysis of fluorescence-activated cell sorting (FACS) crypt populations (Muñoz et al., 2012) revealed that the enterocyte differentiation marker alkaline phosphatase intestinal (*Alpi*) was absent in *Lgr5^{high}* cells, but showed low, yet detectable levels in *Lgr5^{low}* early offspring (Figure 1A). *Alpi* is highly expressed in mature small intestinal enterocytes and encodes the alkaline phosphatase enzyme involved in lipid absorption, pH regulation, and the attenuation of inflammation via detoxification of lipopolysaccharide. Of note, *Alpi^{-/-}* mice are viable and fertile (Narisawa et al., 2003).

In situ hybridization analysis confirmed high-level expression in villus enterocytes (Figure 1B), and low yet detectable expression in cells in the upper crypt. Single-molecule fluorescence in situ hybridization (FISH) analysis for *Alpi* and *Lgr5* confirmed that *Alpi* transcripts in the crypts do not co-localize with *Lgr5* transcripts at the crypt bottom, implying that *Alpi* is not expressed in *Lgr5* stem cells (Figures 1C, 1E, and 1F). *Alpi* transcripts were observed in most cells from cell position +6 or +7 upward (Figure 1D), coinciding with *Ki67⁺* (Figures S1A and S1B) transit-amplifying (TA) cells (Itzkovitz et al., 2012), implying that *Alpi⁺* enterocyte progenitors are proliferative and comprise the bulk of the TA zone. Furthermore, single-molecule FISH for *Alpi* and *Dll1* showed that *Alpi* transcripts do not localize with *Dll1* transcripts located at the +4/+5 position from the crypt base (Figures S1C and S1D), implying that *Alpi⁺* progenitors are distinct from *Dll1⁺* secretory progenitors.

Generation of an Inducible Enterocyte-Specific Cre Line

To generate an enterocyte-specific Cre-line, we inserted an internal ribosome entry site (IRES)-CreERT2 cassette at the stop

codon located in the last exon of the *Alpi* gene (Figure S2A). This strategy involves the endogenous poly-A signal and the 3'UTR of the *Alpi* gene. To characterize Cre activity of the *Alpi^{CreER}* allele, mice were crossed to *R26^{R^{LacZ}}* reporter mice where the *LacZ* gene (whose expression is visualized by X-GAL staining) is under the control of the ubiquitous *Rosa26* (*R26*) locus (Soriano, 1999). 8- to 12-week-old mice were injected with a single dose of tamoxifen (TAM), and killed at various time points for X-GAL analysis. As expected, X-GAL⁺ cells were observed exclusively in enterocytes in the villus domains of the proximal small intestine (Figures 2A–2D) but never in Paneth cells, in villus goblet cells, or in enteroendocrine cells (Figures S3A and S3B). Immunostaining for the estrogen receptor (fused to the Cre moiety) was also restricted to villus enterocytes (Figure S3C), in agreement with *LacZ* expression. At the earliest time point, X-GAL⁺ cells were detected in the upper crypt, but never in the bottom half (i.e., below the +8 position from the crypt bottom) (Figures 2A and 2H). Fewer X-GAL⁺ cells could be detected in crypts 48 hr and 72 hr post-TAM induction (Figures 2C and 2H). X-GAL⁺ cells on days 3 and 4 post-TAM injection were exclusively in the villus domain with day 4 having fewer labeled cells, all in the higher regions of the villi (Figures 2E and 2F). Nearly all X-GAL⁺ cells disappeared within 6 days with occasional single-labeled cells at the top of the villus. Importantly, no labeled cells (be it single cells or clones) were detected 28 days after TAM injection (Figure 2G). No X-GAL staining was ever observed in non-induced mice.

As further proof of bona fide tracing of *Alpi⁺* cells, we used an additional fluorescent reporter line (*Rosa^{tdTomato}*) to follow *Alpi⁺* cells during homeostasis. Similar to labeling with the *LacZ*-reporter, *Alpi^{CreER+/-};Rosa^{tdTomato+/-}* mice injected with TAM showed *tdTomato⁺* *Alpi*-expressing cells in the upper crypt reaches and villus enterocytes but never at the crypt bottom (Figures S3F and S3G). Notably, labeled *Alpi;tdTomato⁺* cells could be detected in both the proximal and distal small intestine (Figures S3F and S3G, respectively) with labeling frequency higher in the proximal, corresponding to higher *Alpi*

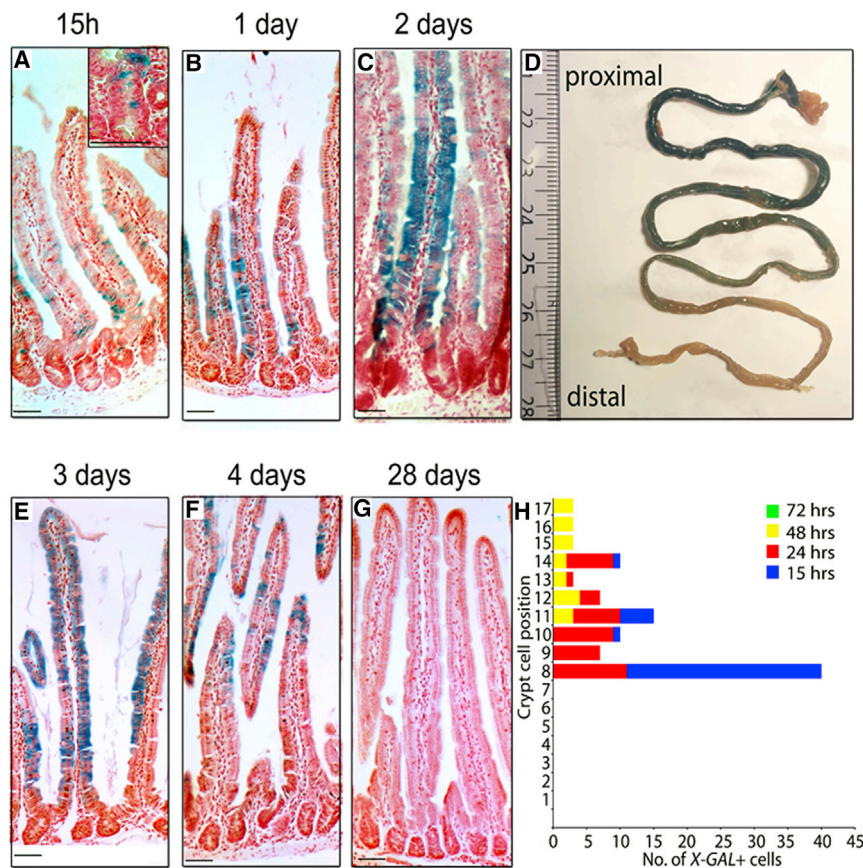


Figure 2. Histological Analysis of LacZ Activity in $Alpi^{CreER}$ KI

(A–G) Mice were induced with 5 mg/kg 4OH-tamoxifen (TAM) and then killed after (A) 15 hr, (B) 1 day, (C) 2 days, (E) 3 days, (F) 4 days, and (G) 28 days. Whole mount X-GAL staining of intact intestine of $Alpi^{CreER};R26R^{LacZ}$ mice showed X-GAL⁺ cells localized to the proximal intestine (duodenum and jejunum) 2 days post-TAM induction. 15 hr post-TAM induction, the majority of the labeled cells were located in the villus. However, labeled cells were observed in the upper crypt level ranging from the +8 position to crypt-villus junction.

(H) Few labeled cells lingered in the upper crypt region 2 days post-TAM induction (representative quantification of X-GAL⁺ crypt cells for 100 crypts). Of note, no labeled cells were detected at the bottom of the crypts. By day 2, labeled cells had almost reached the villus tip. By day 3, labeled cells had reached the tips. By day 4, labeled cells were observed only on the upper half of the villus, implying that most of the labeled cells had completed their life cycle, being shed in the lumen. No labeled cells were observed 28 days post-TAM induction, implying that $Alpi$ is not expressed in stem cells (magnification, 50 μ m). See also Figures S2 and S3.

mRNA expression in the proximal small intestine (Figures S3D and S3E).

$Alpi^+$ Enterocytes Dedifferentiate into Stem Cells upon Depletion of $Lgr5^+$ Stem Cells In Vivo

We next investigated whether absorptive $Alpi$ -expressing enterocytes were capable of conversion into $Lgr5^+$ crypt stem cells. To do so, we crossed $Alpi^{CreER/+};R26R^{LacZ/+}$ mice with $Lgr5^{DTR-GFP/+}$ mice (Tian et al., 2011). In these mice, injection of diphtheria toxin (DT) will cause depletion of $Lgr5^+$ stem cells as well as $Lgr5^+$ quiescent secretory progenitors residing around the +4 position (Buczacki et al., 2013). $Alpi^{CreER/+};R26R^{LacZ/+};Lgr5^{DTR-GFP/+}$ mice were treated simultaneously with TAM and DT and their duodenum were analyzed by X-GAL staining 14 days post-injection (Figure S4A). As controls, we used $Alpi^{CreER/+};R26R^{LacZ/+}$ mice also treated with TAM and DT. Whole-mount X-GAL staining and subsequent histological analysis of $Alpi^{CreER/+};R26R^{LacZ/+};Lgr5^{DTR-GFP/+}$ mice revealed many contiguous ribbons of X-GAL⁺ cells emanating from crypt bottoms and extending up toward adjacent villi (Figure 3C; Figures S4C and S4E) (between 500 and 900 ribbons per mouse). Significantly, no tracing events could be observed in the control mice (Figures 3A, 3B, and 3E). Similar results were obtained when Cre expression was induced 1 day before DT administration, albeit at a somewhat lower frequency (200–300 tracing events per mouse; Figures S4B, S4D, and S4F).

labeled $Alpi^+$ cells were rarely detected in control $Alpi^{CreER/+};Rosa^{tdTomato/+}$ mice after a 6-day chase period (Figure 4A). Importantly, no ribbons were evident in control $Alpi^{CreER/+};Rosa^{tdTomato/+}$ mice injected with TAM and DT (Figure 3E). However, numerous $tdTomato^+$ ribbons along the crypt-villus axis could be observed upon stem cell deletion using $Alpi^{CreER/+};Rosa^{tdTomato/+};Lgr5^{DTR-GFP/+}$ mice (one example given in Figure 3F) with observable co-localization of $tdTomato$ and GFP at crypt bottoms (Figure 3I), corroborating the $R26R^{LacZ}$ reporter analysis that $Alpi^+$ enterocytes dedifferentiate into $Lgr5^+$ stem cells during crypt regeneration.

Contiguous X-GAL⁺ ribbons were still detected in crypt-villus units in $Alpi^{CreER/+};R26R^{LacZ/+};Lgr5^{DTR-GFP/+}$ mice after 3 months (Figures 3G and 3H). These ribbons were positive for GFP expressed by $Lgr5^+$ stem cells (Figure 3I), and contained Paneth, enteroendocrine, and goblet cells of the secretory lineage (Figures 3J–3L) implying that dedifferentiated $Alpi^+$ cells exhibited the $Lgr5^+$ stem cell characteristics of self-renewal and multipotency.

$Alpi^+$ Enterocytes Dedifferentiate into Stem Cells upon Depletion of $Lgr5^+$ Stem Cells In Vitro

To determine whether this plasticity also occurred in vitro, ex-vivo organoid cultures derived from $Alpi^{CreER/+};R26R^{LacZ/+};Lgr5^{DTR-GFP/+}$ crypts were treated with 4-hydroxytamoxifen and DT for 24 hr and analyzed after 4 days (Figure 3M). X-GAL staining on organoids showed X-GAL⁺ cells in crypt domains

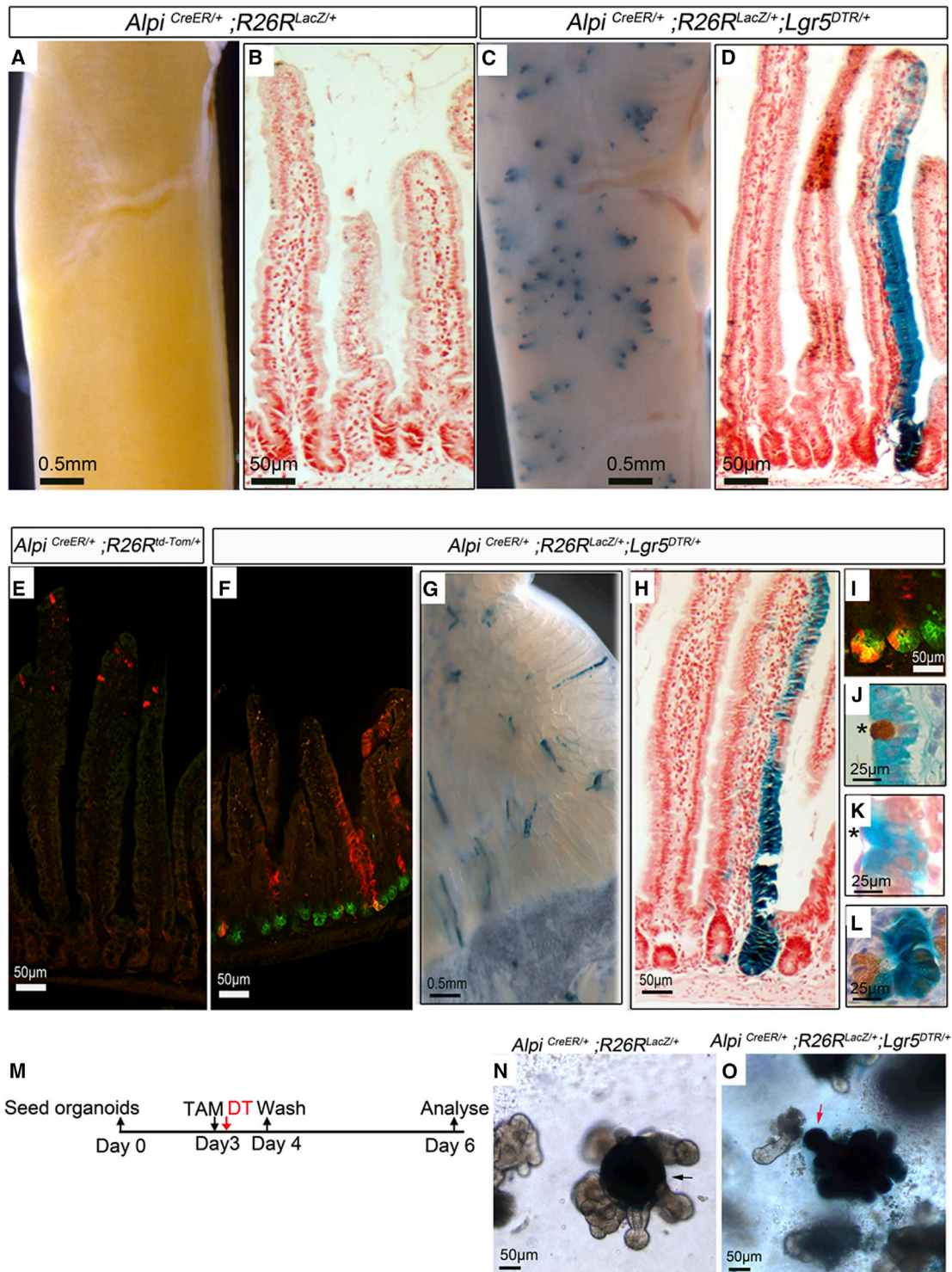


Figure 3. *Alpi*⁺ Enterocytes Dedifferentiate upon Depletion of *Lgr5* Stem Cells

(A and B) *Alpi*^{CreER/+}; *R26R*^{LacZ/+} (control), and *Alpi*^{CreER/+}; *R26R*^{LacZ/+}; *Lgr5*^{DTR-GFP/+} mice were given a single injection each of 5 mg/kg TAM and 50 μg/kg DT and harvested after 2 weeks. X-GAL-stained proximal intestine (A) whole-mount and (B) histological section showing no staining in control group. (C and D) Whole-mount staining and histological section of X-GAL-stained proximal intestine showing X-GAL⁺ crypt/villus units in stem cell depleted group. (E and F) Confocal images of proximal intestine sections from *Alpi*^{CreER/+}; *Rosa*^{tdTomato/+} (control) and *Alpi*^{CreER/+}; *Rosa*^{tdTomato/+}; *Lgr5*^{DTR-GFP/+} mice given a single injection each of 5 mg/kg TAM and 50 μg/kg DT and harvested after 6 days. *Alpi*⁺ cells (red) could not be detected in crypts of control animals (E). (F) Detection of *Alpi*⁺ cells at crypt bottom and red fluorescent stem cell tracings along crypt-villus axis in stem cell depleted mice.

(legend continued on next page)

of stem cell-depleted organoids, but not in crypt regions of $Alpi^{CreER+/+};R26R^{LacZ+/-}$ organoids, which had restricted *LacZ* expression in the central villus domain only (Figures 3N and 3O).

Loss of Dedifferentiation Capacity of $Alpi^+$ Enterocytes upon Crypt Exit

The rapid migration of enterocytes out of the crypts and up toward the villus as they differentiate may diminish their dedifferentiating capacity and reduce their participation in regeneration upon damage to the stem cell pool. To determine at what point this dedifferentiation capacity is lost, induction of $Alpi^+$ cell tracing was initiated 2 and 3 days before deletion of *Lgr5*⁺ stem cells (Figure S5B); at these time points, we expected most if not all of the labeled enterocytes to have migrated out of the crypts. Even lower numbers of X-GAL⁺ crypts (49 tracing events/mouse) were counted when $Alpi^{CreER+/+};R26R^{LacZ+/-};Lgr5^{DTR-GFP+/-}$ mice were injected with TAM 2 days before stem cell depletion (Figures S5B, S5G, and S5H). When these mice were injected with TAM 3 days before induction of stem cell loss virtually no stem cell tracings were observed (Figures S5D and S5H), implying that labeled $Alpi^+$ enterocytes that have exited the crypts after 3 days are no longer proliferative, and do not have the capacity to dedifferentiate to replenish stem cell loss.

Dedifferentiating $Alpi^+$ Cells Turn on Regeneration-Associated Genes

To characterize the transcriptome of $Alpi^+$ cells, we used single-cell sequencing of short-term-labeled $Alpi^+$ cells during homeostasis as well as upon loss of *Lgr5*⁺ stem cells (regeneration). Control *tdTomato*⁺ crypt single cells from $Alpi^{CreER+/-};Rosa^{tdTomato+/-}$ line injected with only TAM (representing homeostasis) and single cells from intestinal crypts of $Alpi^{CreER+/-};Lgr5^{DTR-GFP+/-};Rosa^{tdTomato+/-}$ line singly injected with TAM/DT (representing regeneration) were isolated 24 hr after injection. Thereafter, *tdTomato*⁺ cells from control crypts and *tdTomato* (*Tom*)⁺/*GFP*⁺ from stem-cell-depleted crypts were collected by FACS and sequenced by a modified version of the CEL-seq method (Grün et al., 2015 and references therein). RACE ID analysis (Grün et al., 2015) identified one cluster (cluster 1) from control crypts and four clusters (clusters 4, 3, 2, and 5) from sorted *tdTomato*⁺/*GFP*⁺ cells from stem-cell-depleted crypts (Figures 4A and 4B).

As expected, crypt cells from cluster 1 (Figure 4C) representing $Alpi^+$ enterocyte progenitors during homeostasis were enriched for enterocyte-specific transcripts such as *Apoa1* and *Fabp2* (Figure S6A). In stem-cell-depleted crypts, cells from cluster 4 were also enriched for enterocyte-specific genes

such as *Alpi* and *Fabp1* (Figures 4C and 4D). However, the transcriptome was markedly different from enterocytes in homeostasis because the two populations did not cluster together. In particular, cluster 4 enterocytes were additionally enriched for genes such as *Fth1* (Figure S6B), which is critical for protecting against mucosal damage.

Dedifferentiating $Alpi^+$ Cells Generate Proliferative Cells and Paneth-like Cells

Analysis of cluster 3 (Figures 4B and 4C) showed an enrichment of transcripts for ribosomal proteins (a measure of proliferation) (Grün et al., 2015) (Figure 4D). This proliferative cluster 3 had reduced expression of enterocyte specific gene transcripts, and upregulation of intestinal stem cell specific genes *Ascl2* (van der Flier et al., 2009a), *Smoc2* ($p = 0.004$) and *Cdca7* ($p = 0.004$) (Muñoz et al., 2012) (Figures 4D and S6C). Genes enriched in cluster 3 (such as *Eef1a1*, *Ptma*, and *Slc12a2* and *Ctca4*; Figure 4E) may represent novel genes that are involved in the regenerative process, proliferation, or stem cell identity. Unexpectedly, cluster 2 was enriched for Paneth-cell-specific transcripts such as *Lyz1*, *Defa17*, and *Mmp7* (Figures 4D and S6D). Of note, transcripts for non-*Lgr5*⁺ stem cells with regenerative capacity such as *Dll1* and *Bmi1* were not detected in $Alpi^+$ cells in all clusters, although a few cells showed expression of *Hopx* (Figure S6E). The exact identity of cluster 5, the smallest population, was unclear although they were enriched for genes such as *Hsp90b1* and *ApoE* which mark recently identified rare secretory cells that reside in the crypts (Grün et al., 2015), as well as some enterocyte-specific genes. Nonetheless, this analysis shows that the dedifferentiation reported in this study stems from bona fide enterocyte-lineage cells in intestinal crypts and involves rapid generation of Paneth-like cells.

Apc/Kras Mutated Enterocytes Do Not Form Tumors In Vivo

Recent studies have suggested that differentiated villus epithelial cells can give rise to tumors upon β -catenin/*Kras* mutations (Schwitalla et al., 2013) or overexpression of the BMP antagonist *Grem1* (Davis et al., 2015). However, it is unclear which specific differentiated cells initiate the tumors because the mouse models used (*Xbp1*^{Cre} and *Villin*^{CreER}) have ubiquitous *Cre* expression in all non-*Lgr5*-expressing cells. We thus investigated the tumor-initiating propensity of enterocytes upon *Apc* and *Kras* mutations using the $Alpi^{CreER}$ mouse model.

In line with previous studies where deletion of floxed *Apc* in non-stem cells does not lead to adenoma formation (Barker et al., 2009; Westphalen et al., 2014), no adenomas were detected in $Alpi^{CreER+/+};Apc^{flox/flox}$ mice 28 days after TAM injection

(G and H) Whole-mount staining (G) and histological section (H) of X-GAL⁺ crypt villus units after long term analysis (3 months) signifying self-renewal of $Alpi^+$ dedifferentiated cells.

(I) Co-localization of *tdTomato* (red) from $Alpi^+$ cells and *GFP* (green) from *Lgr5*⁺ cells at crypt bottom showing dedifferentiated $Alpi^+$ enterocytes into stem cells. (J-L) Secretory cells derived from dedifferentiated $Alpi^+$ cells (depicted with asterix); Co-staining of X-GAL with secretory cell markers in $Alpi^{CreER+/+};R26R^{LacZ};Lgr5^{DTR-GFP+/-}$ mice dosed with a single injection of both TAM/DT and killed 3 months post-induction shows that dedifferentiated $Alpi^+$ cells give rise to *Muc2*⁺ goblet cells (J), *ChrgA*⁺ enteroendocrine cells (K), and *Lyz1*⁺ Paneth cells (L).

(M-O) Experimental strategy for in vitro enterocyte plasticity; organoids from $Alpi^{CreER+/+};R26R^{LacZ+/-}$ (control); and $Alpi^{CreER+/+};R26R^{LacZ+/-};Lgr5^{DTR-GFP+/-}$ crypts were seeded for 3 days, treated with 10 nmol/l 4OHT and 0.04 ng/ μ l DT, washed after 24 hr, and X-GAL-stained after 4 days. Control organoids showed X-GAL staining only in the villus domain (black arrow) (N), whereas X-GAL staining occurred in both villus and stem cell domains (red arrow) of stem cell depleted organoids (O).

See also Figure S4.

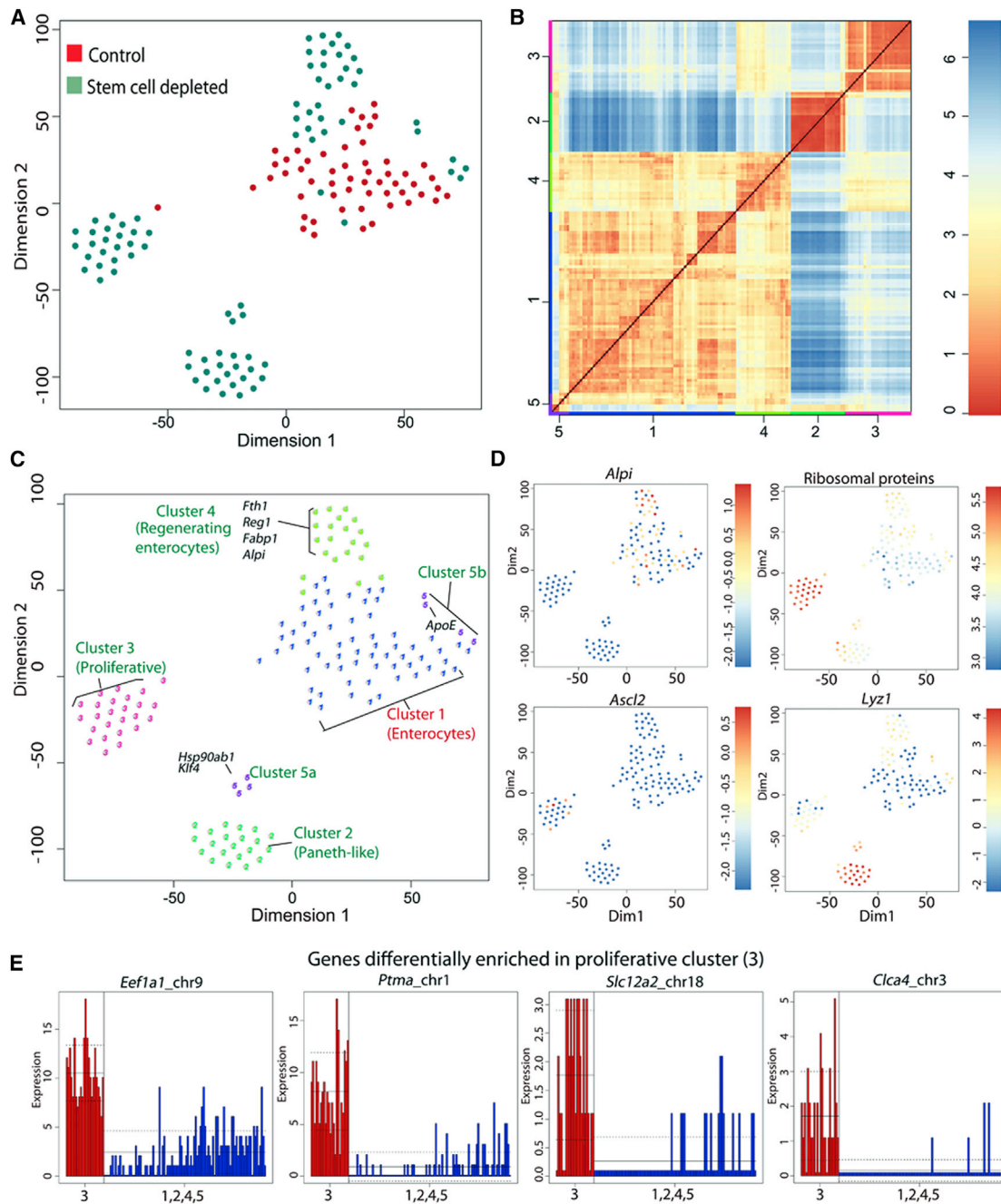


Figure 4. Single-Cell Analysis of Dedifferentiation of *Alpi*⁺ Cells

(A–C) Single cells from crypts from *Alpi*^{CreER+/−};*Rosa*^{tdTomato+/−} mouse injected with TAM (control) and *Alpi*^{CreER+/−};*Rosa*^{tdTomato+/−};*Lgr5*^{DTR-GFP+/−} injected with DT/TAM (stem cell depleted) were analyzed by RACE ID (A) Distribution of cells isolated from control (red) or stem cell depleted (green) animal on a t-SNE map. (B) Heatmap showing k-means clustering of Pearson correlation of transcriptomes of the cells analyzed. (C) Color-coded t-SNE plot displaying cell clusters identified by RaceID.

(D) Distribution of marker gene expression depicted by color-coded t-SNE maps. Color bars on right indicate expression levels as log₂ transformed normalized counts. *Alpi* is restricted to clusters 1, 4, and 5, which are the putative enterocytes. Cluster 3 displays high ribosomal gene expression associated with proliferation (upper left) and the stem cell marker *Asc2* (lower left). Cluster 2 expresses high levels of Paneth cell genes (upper right).

(E) Barplots showing some of the differentially expressed genes specific to the proliferative cluster 2.

See also Figure S5.

(Figures 5A and 5B). Oncogenic *Kras* synergistically enhances Wnt hyperactivation upon *Apc* deletion and thus tumor progression in the intestine (Janssen et al., 2006). We generated

Alpi^{CreER+/−};*Apc*^{flox/flox};*Kras*^{LSL G12D+/−} mice to mutate both *Apc* and *Kras* specifically in enterocytes. Surprisingly, combined mutations of both *Apc* and *Kras* in enterocytes did not cause

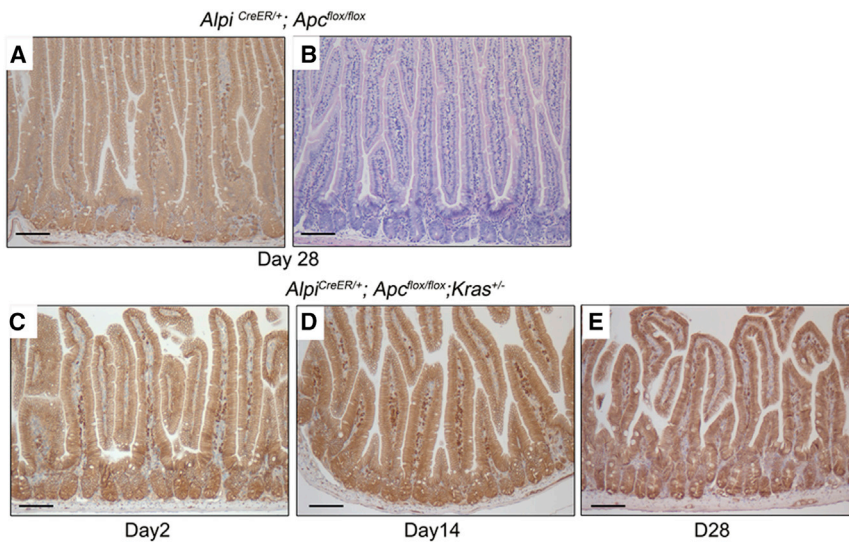


Figure 5. *Apc* and *Apc/Kras* Mutations in Enterocytes

(A and B) Nuclear β -catenin staining (A) and H/E staining (B) of $Alpi^{CreER+/+}; Apc^{flox/flox}$ mouse injected with a single dose of tamoxifen and sacrificed after 28 days showing no adenoma formation or morphological aberrations in the proximal small intestine.

(C–E) $Alpi^{CreER+/+}; Apc^{flox/flox}; Kras^{LSL G12D+/-}$ animals were injected with a single dose of 5 mg/ml and killed at various times and sacrificed after 28 days showing no adenoma formation or morphological aberrations in the proximal small intestine. No accumulation of nuclear β -catenin at 2 days (C). No adenomas were observed at later time points: 14 days (D) and 28 days (E).

nuclear accumulation of β -catenin (Figure 5C) or yielded any adenomas in vivo 2 weeks and 28 days after TAM injection (Figures 5D and 5E).

***Apc/Kras*-Mutated Enterocytes Form Tumor Organoids In Vitro**

We next investigated whether mutated enterocytes have the capacity to dedifferentiate ex vivo and exhibit cancer stem cell properties. Crypts and villi were isolated from $Alpi^{CreER+/+}; R26R^{LacZ+/-}; Apc^{flox/flox}$ and $Alpi^{CreER}; R26R^{LacZ+/-}; Apc^{flox/flox}; Kras^{LSL G12D+/-}$ compound mutants, 2 days after TAM injection and cultured in organoid growth medium (ENR) (Figures S6A and S6B). Isolated crypts from *Apc*-deleted enterocyte progenitors did not form spherical organoids (Figure 6C) characteristic of hyperactive Wnt-triggered cells. However, a significant number of $X-GAL^+$ spherical organoids could be observed in *Apc/Kras* mutated crypts (Figures S6D and S6E). These tumor organoids could be cultured for weeks independent of EGF, Noggin and Rspodin1 required for normal organoids but dispensable for *Apc* mutant/*Kras* mutant organoids (Drost et al., 2015) (Figures S6A–S6D and S6G). Additionally, $Alpi^+$ -derived tumor organoids could be cultured in advanced DMEM/F12 media without n-Acetylcysteine and B27 supplements (Figures S6E and S6F), (essential antioxidant components for normal organoid culture). Villi from both *Apc*-mutated (not shown) and *Apc/Kras*-mutated mice failed to generate spheroid organoids regardless of whether they were cultured as whole villi or single villus cells (Figures 6F and 6G).

DISCUSSION

Combined with previous studies, our current observations underscore the extent of plasticity of crypt progenitors. Previous reports have demonstrated that cycling secretory progenitors (van Es et al., 2012) as well as quiescent secretory precursors (Buczacki et al., 2013) can revert to a multipotent state upon loss of resident $Lgr5^+$ stem cells. We now find that a population that comprises the bulk of the crypt above the stem/Paneth cell niche also displays similar plasticity. Due to the large number of

absorptive progenitors and the higher frequency of dedifferentiating events (as compared to previous *Dll1*+ secretory progenitors) it is likely that these cells may constitute the committed progenitor pool of first choice in intestinal regeneration induced dedifferentiation. Dedifferentiation of enterocytes may also be affected by the mode of injury. Although not probed in this study, it is likely that the regenerative capacity of short-lived proliferative enterocytes may be inhibited by anti-proliferative damage such as irradiation and 5-fluorouracil treatment.

Single cell analysis of $Alpi^+$ crypt cells expressing the *tdTomato* reporter during homeostasis confirmed their identity as enterocyte-lineage progenitors, enriched for various other enterocyte-specific transcripts. Upon injury to the stem-cell compartment, $Alpi^+$ progenitors downregulate enterocyte-specific genes, become more proliferative and upregulate *Lgr5* stem-cell-specific genes.

$Alpi^+$ enterocytes upregulate genes associated with regeneration after injury such as *Fth1*. Production of H-ferritin (*Fth1*) by enterocytes is required for accurate iron absorption that prevents toxic iron overload and iron deficiency (Andrews, 2010; Vanoica et al., 2010). Induction of *Fth1* has been linked to playing a protective role upon acute kidney injury. High iron levels mediate injury by promoting increased generation of reactive oxygen species (Zarjou et al., 2013). A hallmark of cell ablation by DT is apoptotic cell death (Buch et al., 2005; Metcalfe et al., 2013; Tian et al., 2011), leading to the release of reactive oxygen species (Circu and Aw, 2010). Expression of genes such as *Fth1* by enterocytes upon damage suggests that in addition to their dedifferentiation function, they might be involved in mitigating oxidative stress from apoptosis.

The unexpected occurrence of Paneth-like cells during regeneration could imply rapid specification of Paneth cells from de novo stem cells derived from dedifferentiating $Alpi^+$ cells to support the regenerative process. Additionally, it is tempting to speculate that during regeneration, $Alpi^+$ enterocytes intestinal crypts can transdifferentiate into Paneth cells or rare secretory cells (cluster 5) (Grün et al., 2015). Further studies are needed to test these hypotheses.

The classical view of an adult stem-cell hierarchy such as defined for hematopoietic stem cells appears not to apply to the crypt. Rather, crypts are populated by multiple committed progenitors that can revert to a stem-cell phenotype when

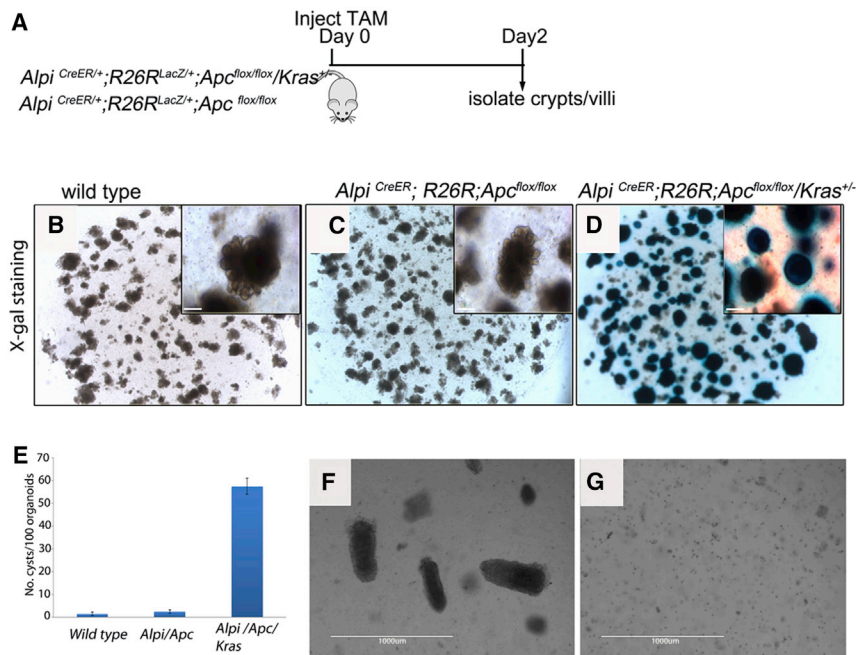


Figure 6. $Alpi^+$ Crypt Cells Form Tumor Organoids In Vitro

(A–D) Scheme to mutate and isolate $Alpi^+$ cells for in vitro organoid assay. $Alpi^{CreER+/+}; R26R^{LacZ+/+}; Apc^{flox/flox}$ and $Alpi^{CreER+/+}; R26R^{LacZ+/+}; Apc^{flox/flox}; Kras^{LSL G12D+/-}$ mice were injected with a single dose of tamoxifen and killed after 2 days for crypt and villi isolation. Controls were wild-type mice ($Alpi^{CreER-/-}$) injected with TAM (B). $Alpi^{CreER+/+}; R26R^{LacZ+/+}; Apc^{flox/flox}$ crypts formed normal organoids (C) comparable to wild-type organoids, whereas $Alpi^{CreER+/+}; R26R^{LacZ+/+}; Apc^{flox/flox}; Kras^{LSL G12D+/-}$ crypts formed spheroid tumor organoids that were X-GAL⁺ (D), indicative of their enterocyte origin. Scale bar in (B)–(D) represents 20 μ m. (E) Spheroid organoid forming efficiency of mutated $Alpi^+$ crypt cells; 50% of $Alpi^{CreER+/+}; R26R^{LacZ+/+}; Apc^{flox/flox}; Kras^{LSL G12D+/-}$ ($Alpi/Apc/Kras$) crypts formed spherical organoids characteristic of tumor organoids after first passage whereas wild-type and $Alpi^{CreER+/+}; R26R^{LacZ+/+}; Apc^{flox/flox}$ ($Alpi/Apc$) crypts did not form spheroid organoids. Error bars represent \pm SD.

(F and G) Isolated villi from $Alpi^{CreER+/+}; R26R^{LacZ+/+}; Apc^{flox/flox}; Kras^{LSL G12D+/-}$ were isolated and embedded into Matrigel whole (F) or single cells (G), but failed to grow into spherical tumor organoids. Scale bar represents 1,000 μ m. See also Figure S6.

exposed to the niche at the crypt bottom. Similar mechanisms of daughter cell plasticity is emerging in other epithelial systems, i.e., the dedifferentiation of committed mature airway cells in the lung (Tata et al., 2013), and of *Troy*⁺ chief cells in the gastric corpus (Stange et al., 2013). A plausible explanation for the observed enterocyte plasticity could rest in a permissive epigenetic state in enterocyte precursors. Recent studies on DNA methylation and histone marks in intestinal crypt/villus cells revealed the virtual absence of differences between *Lgr5*⁺ stem cells and committed enterocytes precursors (Kim et al., 2014; Kaaij et al., 2013), in striking contrast to the situation in the hematopoietic stem cell hierarchy (Hogart et al., 2012; Hodges et al., 2011; Ji et al., 2010), implying that the chromatin in enterocytes is permissive for rapid reprogramming into *Lgr5*⁺ stem cells during regeneration.

Deletion of *Apc* triggers hyperactive *Wnt* signaling that transforms *Lgr5*⁺ stem cells (but not non-stem cells in crypts and villi) into tumor initiating cells (Barker et al., 2009). Loss of *Apc* in combination with depletion of *Lgr5*⁺ stem cells causes crypt hyperplasia presumably from crypt cells within the *Lgr5*⁻ population (Metcalfe et al., 2013). Furthermore, recent studies have suggested β -catenin/*Kras* mutations (Schwitalla et al., 2013) and *Grem1* overexpression in non-*Lgr5*-expressing cells (Davis et al., 2015) can lead to tumor formation although the exact identity of the tumor-initiating cells was not probed in these studies. In contrast to these studies, we did not observe tumors in vivo from *Apc* or *Apc/Kras*-mutated enterocyte progenitors. That *Apc*-mutated enterocyte progenitors failed to generate tumor organoids ex vivo suggests the differentiation state or the short-lived nature of enterocyte progenitors suppresses tumorigenic transformation upon deletion of *Apc*.

$Alpi^+$ *Apc/Kras*-mutated crypt cells did form spherical “tumor organoids” in ex vivo 3D Matrigel cultures without growth factors

that are normally required for stem cell maintenance, in agreement with previous studies (Drost et al., 2015; Matano et al., 2015). In vivo, the short residence time of enterocyte progenitors in the crypts might prevent combined *Apc/Kras* mutations from being fixed in the crypts to cause cancer. This supports the notion that the architecture of the small intestine crypt/villus domain suppresses the fixation of tumorigenic $Alpi^+$ cells (Vermeulen et al., 2013). Ex vivo, the architectural and time restraints on mutated $Alpi^+$ cells are removed, allowing time and unlimited access to niche factors that support tumorigenic transformation. Thus, the short-lifespan of enterocyte progenitors and their rapid migration rate out of crypts might play a protective role against tumorigenesis. Indeed, cancers are very rare in the proximal small intestine (Goldner and Stabile, 2014).

In contrast to reported tumorigenesis from villus enterocytes upon β -catenin/*Kras* mutations using the *Xbp1*^{CreER} reporter, and *Grem1* overexpression using the *Villin*^{CreER} reporter, we did not observe tumors from villus enterocytes with our $Alpi$ ^{CreER} reporter upon *Apc/Kras* mutations. Because *Xbp1* and *Villin* expression are not exclusive to enterocytes, it is likely that tumors in these models did not originate from enterocytes.

Taken together, our data demonstrate that short-lived $Alpi^+$ enterocyte progenitor cells can dedifferentiate and act as reserve stem cells to replenish loss of *Lgr5*⁺ stem cells, to play a protective role upon injury. Thus, “stemness” does not appear to be an intrinsic, “hard-wired” property of rare stem cells (Clevers, 2015), but can be imposed on multiple different progenitors by the stem cell niche.

EXPERIMENTAL PROCEDURES

All animal procedures and experiments were performed in accordance with national animal welfare laws under a project license obtained from the Dutch

Government, and were reviewed by the Animal Ethics Committee of the Royal Netherlands Academy of Arts and Sciences (KNAW).

Generation of Mice and Mouse Experiments

Lgr5^{DTR-GFP} mice have been previously described (Tian et al., 2011).

Knockin construct for generation of *Alpi*^{CreER} mice was assembled according to the diagram in Figure S2A. Oligonucleotides used for targeting arms are given in Tables S1A and S1B. One hundred micrograms of the targeting construct was linearized and transfected (800V; 3F) into embryonic stem (ES) cells derived from 129/Ola-derived IB10 strain. Recombined ES clones expressing the neomycin gene were selected in G418 (200 g/ml) supplemented medium.

Southern blot analysis (Figure S2B) with a probe upstream of the targeted region confirmed precise homologous recombination in approximately five of 100 ES clones. Southern blot probe oligonucleotides are given in Table S1C.

Two independent positive clones were injected into C57BL/6 blastocysts according to standard procedures. The neomycin selection cassette flanked by FRT sites was excised in vivo by crossing the mice with FLP1 mice.

Heterozygous and homozygous mice (Figure S2C) were retrieved at the expected Mendelian ratios at birth, and adult transgenic animals showed no discernible abnormality, with comparable lifespan and fertility compared to wild-type littermates. Genotyping primers are provided in Table S1D.

R26R^{LacZ} (Soriano, 1999) and *Rosa*^{tdTomato} (Madisen et al., 2010) Cre reporter mice were obtained from the Jackson Laboratory. Eight- to 14-week-old mice were injected intraperitoneally with 5 mg/kg of TAM and 50 µg/kg DT.

Alpi^{CreER+/+}; *R26R*^{LacZ+/-} mice were bred with *Apc*^{flox/flox} and *Kras*^{LSL G12D+/-} mice to generate *Alpi*^{CreER+/+}; *R26R*^{LacZ} *Apc*^{flox/flox}; *Kras*^{LSL G12D+/-} mice or *Alpi*^{CreER+/+}; *R26R*^{LacZ}; *Apc*^{flox/flox} mice. Six- to 14-week-old mice were used for all experiments. A single dose of 5 mg/ml TAM was injected intraperitoneally to activate Cre-mediated mutation of *Apc* and/or *Kras* in *Alpi*⁺ cells. A total of five mice were injected for each experimental group. As controls, we used *Alpi*^{CreER} mice given similar doses of TAM.

X-gal Staining

Proximal intestines isolated from mice were fixed for 2 hr on ice with fix solution (1% paraformaldehyde [PFA], 0.2% glutaraldehyde, and 0.02% NP40 in PBSO), and washed twice for 15 min in PBSO. This was followed by overnight staining in the dark with 1 mg/ml X-gal in PBSO solution containing 5 mmol/l potassium-hexacyanoferrate III, 5 mmol/l potassium-hexacyanoferrate (IV) trihydrate, 2 mmol/l magnesium chloride, 0.02% NP40, and 0.1% sodium deoxycholate. Subsequently, tissues were washed twice in PBSO and whole-mount analyzed for X-GAL positivity followed by overnight fixation in 4% PFA, and paraffin embedding using standard procedures. Four to 8 µm tissue sections were counterstained with neutral red. Three mice per each experimental group were used for analysis.

Immunohistochemistry

Mice tissues were fixed in 4% PFA overnight, paraffin embedded, and sectioned at 4–10 µm. Immunohistochemistry was carried out as previously described (Barker et al., 2007) using the following antibodies for immunostaining: rabbit anti-*ChrgA* (1:500, Santa Cruz, sc-1488); anti-estrogen receptor (ER, 1:500, Abcam, ab27595) anti-*β-catenin* (1:100; Transduction Lab, Product number 610154), and anti-Lysozyme 1 (Dako, 1:1,500, A009902).

Briefly, tissues on paraffin sections were dewaxed in xylene for 5 min, hydrated in ethanol (2 × 1 min in 100% ethanol, 2 × 1 min in 96% ethanol, 2 × 1 min in 70% ethanol), and rinsed three times with demi water. Endogenous peroxidase was blocked by submerging sections in buffer containing citric acid and disodium-hydrogen phosphate-2-hydrate for 15 min followed by rinsing with demi water. This was followed by antigen retrieval using TRIS-EDTA (pH 9.0) or citrate, according to the antibody manufacturer's instructions. Sections were then blocked with 0.05% BSA/PBS solution for 30 min, followed by antibody staining at concentrations indicated above, 2 hr at room temperature or 4°C overnight. In all cases, reagent from the Envision+ kit (Dako) was used as a secondary reagent. Stainings were then developed with DAB. Slides were counterstained with hematoxylin and mounted.

In Situ Hybridization

In situ hybridization probe targeting *Alpi* was generated by PCR from whole-intestine cDNA using the oligonucleotides given in Table S1E, with the antisense primer tethered to T3 promoter sequence. Tissue preparation and hybridization procedures were as previously described (van der Flier et al., 2009b). Briefly, paraffin tissue sections on glass slides were first dewaxed in xylene for 15 minutes, then in ethanol series (100%, 75%, 50%, 25%, 5 min in each), and rinsed in DEPC-treated water for 10 min. Slides were then treated with 0.2N HCl for 15 min, rinsed, and incubated with 30 µg/ml Proteinase K in PBS for 20 min at 37°C. Slides were then rinsed with 0.2% glycine/PBS, PBS, post-fixed with 4% PFA for 10 min, and rinsed. Thereafter, slides were incubated with acetic anhydride solution (50 ml deionized water, 300 µl acetic anhydride, 670 µl triethanolamine, and 200 µl concentrated HCl), for 5 min, then washed with PBS and 5XSSC. Slides were then pre-hybridized for 2 hr at 70°C, followed by incubation with Digoxigenin-labeled probe in hybridization buffer overnight. Thereafter, slides were washed with 2XSSC solution and washed three times for 20 min at 62°C in 2XSSC/50% formamide solution. This was followed by washing in tris buffered saline containing 0.1% Tween detergent (TBST), and blocking with 0.5% blocking powder in TBST, for 30 min. Thereafter, slides were incubated with sheep anti-digoxigenin Fab (Roche) 1:2,000 in blocking solution overnight at 4°C. Slides were washed in NTM buffer (1M Tris [pH 9.5], 0.05M MgCl₂, 0.1M NaCl) followed by incubation with NBT/BCIP overnight for colorimetric development of alkaline phosphatase activity. Slides were then washed, fixed, and mounted.

Microarray Data Analysis

Microarray analysis was performed with data uploaded on the R2: microarray analysis and visualization platform (<http://r2.amc.nl>) (R2 internal identifier: ps_wetering_coloexp24_htmg430pm).

Single-Molecule FISH

Probe library for *Alpi* were designed and constructed as previously described. Library consisted of 48 probes of length 20 base pairs, complementary to the coding sequence of *Alpi*. *Lgr5*-Cy5 probe was a kind gift from Anna van Oudenaarden. Tissue processing and hybridization procedures were according to protocol described in (Lyubimova et al., 2013). Briefly, hybridizations were carried out overnight with *Lgr5* labeled Cy5 probe and Alexa 594 labeled *Alpi* probe. DAPI dye was added to washing buffer followed by counterstaining with *Phalloidin*. Images were taken with a Leica MM-AF fluorescence microscope equipped with a 100× oil-immersion objective and a Princeton Instruments camera using Metamorph software (Molecular Devices). Image-plane pixel dimensions were 0.13 µm. Quantification of transcripts in ten crypts, was carried out on 20 stacks with a Z spacing of 0.3 µm. Image processing was done with ImageJ software, using the variance filter and background subtraction filter for image enhancement.

Single-Cell Sequencing

Alpi^{CreER+/-}; *Rosa*^{tdTomato+/-} injected with TAM and *Alpi*^{CreER+/-}; *Lgr5*^{DT-GFP+/-}; *Rosa*^{tdTomato+/-} mice injected with TAM/DT were killed after 24 hours. Thereafter, crypts were isolated and dissociated into single cells followed by FACS (FACS Arial cell sorter, BD Bioscience) of *tdTomato*⁺ cells into 96-well plates containing 100 µl Trizol (Life Technologies). Total RNA extraction and generation of single-cell RNA expression libraries were performed as described by (Grün et al., 2015 and references therein). A total of 192 cells were sequenced on an Illumina HighSeq 2500 instrument for each group, using 50 base-pair paired end sequencing. K-means clustering was used to delineate clusters of *tdTomato*⁺ cells in homeostasis and regeneration.

Confocal Microscopy

Horizontal whole mounts of intestinal tissues from *Alpi*^{CreER+/-}; *Rosa*^{tdTomato+/-} mice were prepared using a previously described protocol (Driskell et al., 2012, 2013). Briefly, intestinal tissues were fixed for 15 min in 4% PFA, washed in PBS, and then embedded in cryomold. Sections were cut in a cryostat at a thickness of 80 µm and placed in room temperature PBS using forceps, to wash away the OCT. Tissue sections were then mounted on glass slides with a small volume of 100% glycerol and analyzed by confocal microscopy. Microscopy was performed using a Leica SP8 confocal microscope and images were analyzed in Adobe Photoshop CS5.

Organoid Culture

Mouse organoids were established and maintained from isolated crypts of the proximal small intestine as previously described (Sato et al., 2009). Briefly, intestines were cut open along the length. Villi were removed by scraping with a sterile microscope glass slide and separated into two parts. Whole villi were washed in cold PBS (without Ca/Mg) and seeded in Matrigel with either organoid medium (ENR) or Wnt supplemented organoid medium (WENR).

For making single cells from villi, scraped villi were transferred to 30 ml of ice cold PBS + 5mM EDTA in a falcon tube and incubated for 30 min at 4°C with rolling. Tube was then centrifuged at 650 rpm for 5 min and the supernatant carefully removed. Villi were then resuspended in 1 ml SMEM calcium-free medium (GIBCO 11380) and mixed with 1 ml of SMEM with 1 mg/ml Trypsin (Sigma T1426) followed by mixing by pipetting. DNase (final concentration of 1u/ul) was then added to the villi suspension and incubated 10 min at 37°C with intermittent shaking and checking under a microscope for single cells. Suspension was then centrifuged for 5 min at 650 rpm, supernatant discarded, and seeded in Matrigel and subsequently cultured with either ENR or WENR media. Rho kinase inhibitor was added to the culture media in all cases.

To detect β -galactosidase expression *ex vivo*, organoids from $Alpl^{CreER/+}$; $Rosa^{LacZ+/-}$ and $Alpl^{CreER/+}$; $Rosa^{LacZ+/-}$; $Lgr5^{DTR-GFP+/-}$ crypts seeded for 3 days were treated with 4-hydroxytamoxifen (4-OHT; Sigma; 10 nmol/l), or 4-OHT/0.04 ng/ μ l DT, respectively. After 24 hr, media was replaced by normal organoid culture media for 3 days followed by X-GAL staining (as described above for whole intestines), with organoids still in Matrigel.

SUPPLEMENTAL INFORMATION

Supplemental Information includes six figures and one table and can be found with this article online at <http://dx.doi.org/10.1016/j.stem.2016.01.001>.

AUTHOR CONTRIBUTIONS

P.W.T. and H.C. conceived the project. P.W.T. made the $Alpl^{CreER}$ mouse and was supervised by J.v.E. and H.F. O.B. and K.W. generated the single-cell sequencing RNA libraries and analyzed the data, under the supervision of A.v.O. P.W.T., H.B., and J.K. performed histology experiments. P.W.T. and K.K. performed confocal imaging experiments. Mouse handling and injections were carried out by M.v.B. under the supervision of J.H.v.E. P.W.T. generated mouse organoids and performed *in vitro* experiments. F.d.S. contributed the $Lgr5$ -DTR-GFP mouse. P.W.T. and H.C. wrote the manuscript and edited it together with O.B. and H.F.

ACKNOWLEDGMENTS

The authors express their sincere gratitude to Stieneke van den Brink, Nobuo Sasaki, Norman Sachs, Helmuth Gehart, Carla Kroon-Veenboer, Lucas Kaaij, Anna van Oudenaarden, Lennart Kester, Reinier van der Linden, Stefan van der Elst, and Ewart de Bruijn for excellent technical assistance. P.W.T. was supported by a Netherlands Organization for Scientific Research (NWO) personal grant. O.B. was supported by a CBG fellowship. H.F. was supported by an EMBO long-term fellowship. K.K. is supported by long-term fellowships from EMBO and HFSP. K.W. was supported by a European Research Council Advanced grant (ERC-AdG 294325-GeneNoiseControl) and a Nederlandse Organisatie voor Wetenschappelijk Onderzoek (NWO) Vici award. J.H.v.E. was supported by a LEDUCQ-TNE grant. M.v.d.B. and H.B. were supported by CVON-HUSTCARE grants.

Received: November 14, 2014

Revised: November 3, 2015

Accepted: January 4, 2016

Published: January 28, 2016

REFERENCES

Andrews, N.C. (2010). Ferritin(in)ing out new mechanisms in iron homeostasis. *Cell Metab.* 12, 203–204.

Barker, N., van Es, J.H., Kuipers, J., Kujala, P., van den Born, M., Cozijnsen, M., Haegebarth, A., Korving, J., Begthel, H., Peters, P.J., and Clevers, H. (2007). Identification of stem cells in small intestine and colon by marker gene *Lgr5*. *Nature* 449, 1003–1007.

Barker, N., Ridgway, R.A., van Es, J.H., van de Wetering, M., Begthel, H., van den Born, M., Danenberg, E., Clarke, A.R., Sansom, O.J., and Clevers, H. (2009). Crypt stem cells as the cells-of-origin of intestinal cancer. *Nature* 457, 608–611.

Bernal, N.P., Stehr, W., Zhang, Y., Profitt, S., Erwin, C.R., and Warner, B.W. (2005). Evidence for active Wnt signaling during postresection intestinal adaptation. *J. Pediatr. Surg.* 40, 1025–1029, discussion 1029.

Buch, T., Heppner, F.L., Tertilt, C., Heinen, T.J.A.J., Kremer, M., Wunderlich, F.T., Jung, S., and Waisman, A. (2005). A Cre-inducible diphtheria toxin receptor mediates cell lineage ablation after toxin administration. *Nat. Methods* 2, 419–426.

Buczacki, S.J.A., Zecchini, H.I., Nicholson, A.M., Russell, R., Vermeulen, L., Kemp, R., and Winton, D.J. (2013). Intestinal label-retaining cells are secretory precursors expressing *Lgr5*. *Nature* 495, 65–69.

Circu, M.L., and Aw, T.Y. (2010). Reactive oxygen species, cellular redox systems, and apoptosis. *Free Radic. Biol. Med.* 48, 749–762.

Clevers, H. (2013). The intestinal crypt, a prototype stem cell compartment. *Cell* 154, 274–284.

Clevers, H. (2015). STEM CELLS. What is an adult stem cell? *Science* 350, 1319–1320.

Davis, H., Irshad, S., Bansal, M., Rafferty, H., Boitsova, T., Bardella, C., Jaeger, E., Lewis, A., Freeman-Mills, L., Giner, F.C., et al. (2015). Aberrant epithelial *GREM1* expression initiates colonic tumorigenesis from cells outside the stem cell niche. *Nat. Med.* 21, 62–70.

Driskell, R.R., Juneja, V.R., Connelly, J.T., Kretzschmar, K., Tan, D.W.-M., and Watt, F.M. (2012). Clonal growth of dermal papilla cells in hydrogels reveals intrinsic differences between Sox2-positive and -negative cells *in vitro* and *in vivo*. *J. Invest. Dermatol.* 132, 1084–1093.

Driskell, R.R., Lichtenberger, B.M., Hoste, E., Kretzschmar, K., Simons, B.D., Charalambous, M., Ferron, S.R., Herauld, Y., Pavlovic, G., Ferguson-Smith, A.C., and Watt, F.M. (2013). Distinct fibroblast lineages determine dermal architecture in skin development and repair. *Nature* 504, 277–281.

Drost, J., van Jaarsveld, R.H., Ponsioen, B., Zimmerlin, C., van Boxtel, R., Buijs, A., Sachs, N., Overmeer, R.M., Offerhaus, G.J., Begthel, H., et al. (2015). Sequential cancer mutations in cultured human intestinal stem cells. *Nature* 521, 43–47.

Goldner, B., and Stabile, B.E. (2014). Duodenal adenocarcinoma: why the extreme rarity of duodenal bulb primary tumors? *Am. Surg.* 80, 956–959.

Grün, D., Lyubimova, A., Kester, L., Wiebrands, K., Basak, O., Sasaki, N., Clevers, H., and van Oudenaarden, A. (2015). Single-cell messenger RNA sequencing reveals rare intestinal cell types. *Nature* 525, 251–255.

Hodges, E., Molaro, A., Dos Santos, C.O., Thekkat, P., Song, Q., Uren, P.J., Park, J., Butler, J., Rafii, S., McCombie, W.R., et al. (2011). Directional DNA methylation changes and complex intermediate states accompany lineage specificity in the adult hematopoietic compartment. *Mol. Cell* 44, 17–28.

Hogart, A., Lichtenberg, J., Ajay, S.S., Anderson, S., Margulies, E.H., and Bodine, D.M.; NIH Intramural Sequencing Center (2012). Genome-wide DNA methylation profiles in hematopoietic stem and progenitor cells reveal overrepresentation of ETS transcription factor binding sites. *Genome Res.* 22, 1407–1418.

Itzkovitz, S., Lyubimova, A., Blat, I.C., Maynard, M., van Es, J., Lees, J., Jacks, T., Clevers, H., and van Oudenaarden, A. (2012). Single-molecule transcript counting of stem-cell markers in the mouse intestine. *Nat. Cell Biol.* 14, 106–114.

Janssen, K.P., Alberici, P., Fsihi, H., Gaspar, C., Breukel, C., Franken, P., Rosty, C., Abal, M., El Marjou, F., Smits, R., et al. (2006). APC and oncogenic KRAS are synergistic in enhancing Wnt signaling in intestinal tumor formation and progression. *Gastroenterology* 131, 1096–1109.

- Ji, H., Ehrlich, L.I.R., Seita, J., Murakami, P., Doi, A., Lindau, P., Lee, H., Aryee, M.J., Irizarry, R.A., Kim, K., et al. (2010). Comprehensive methylome map of lineage commitment from haematopoietic progenitors. *Nature* **467**, 338–342.
- Kaaij, L.T., van de Wetering, M., Fang, F., Decato, B., Molaro, A., van de Werken, H.J., van Es, J.H., Schuijers, J., de Wit, E., de Laat, W., et al. (2013). DNA methylation dynamics during intestinal stem cell differentiation reveals enhancers driving gene expression in the villus. *Genome Biol.* **14**, R50.
- Kim, T.-H., Li, F., Ferreira-Neira, I., Ho, L.-L., Luyten, A., Nalapareddy, K., Long, H., Verzi, M., and Shivdasani, R.A. (2014). Broadly permissive intestinal chromatin underlies lateral inhibition and cell plasticity. *Nature* **506**, 511–515.
- Lyubimova, A., Itzkovitz, S., Junker, J.P., Fan, Z.P., Wu, X., and van Oudenaarden, A. (2013). Single-molecule mRNA detection and counting in mammalian tissue. *Nat. Protoc.* **8**, 1743–1758.
- Madisen, L., Zwingman, T.A., Sunken, S.M., Oh, S.W., Zariwala, H.A., Gu, H., Ng, L.L., Palmiter, R.D., Hawrylycz, M.J., Jones, A.R., et al. (2010). A robust and high-throughput Cre reporting and characterization system for the whole mouse brain. *Nat. Neurosci.* **13**, 133–140.
- Matano, M., Date, S., Shimokawa, M., Takano, A., Fujii, M., Ohta, Y., Watanabe, T., Kanai, T., and Sato, T. (2015). Modeling colorectal cancer using CRISPR-Cas9-mediated engineering of human intestinal organoids. *Nat. Med.* **21**, 256–262.
- Metcalfe, C., Klijavin, N.M., Ybarra, R., and de Sauvage, F.J. (2013). Lgr5+ stem cells are indispensable for radiation-induced intestinal regeneration. *Cell Stem Cell* **14**, 149–159.
- Montgomery, R.K., Carlone, D.L., Richmond, C.A., Farilla, L., Kranendonk, M.E.G., Henderson, D.E., Baffour-Awuah, N.Y., Ambruzs, D.M., Fogli, L.K., Algra, S., and Breault, D.T. (2011). Mouse telomerase reverse transcriptase (mTert) expression marks slowly cycling intestinal stem cells. *Proc. Natl. Acad. Sci. USA* **108**, 179–184.
- Muñoz, J., Stange, D.E., Schepers, A.G., van de Wetering, M., Koo, B.-K., Itzkovitz, S., Volckmann, R., Kung, K.S., Koster, J., Radulescu, S., et al. (2012). The Lgr5 intestinal stem cell signature: robust expression of proposed quiescent '+4' cell markers. *EMBO J.* **31**, 3079–3091.
- Narisawa, S., Huang, L., Iwasaki, A., Hasegawa, H., Alpers, D.H., and Millán, J.L. (2003). Accelerated fat absorption in intestinal alkaline phosphatase knockout mice. *Mol. Cell. Biol.* **23**, 7525–7530.
- Powell, A.E., Wang, Y., Li, Y., Poulin, E.J., Means, A.L., Washington, M.K., Higginbotham, J.N., Juchheim, A., Prasad, N., Levy, S.E., et al. (2012). The pan-ErbB negative regulator Lrig1 is an intestinal stem cell marker that functions as a tumor suppressor. *Cell* **149**, 146–158.
- Sangiorgi, E., and Capecchi, M.R. (2008). Bmi1 is expressed in vivo in intestinal stem cells. *Nat. Genet.* **40**, 915–920.
- Sato, T., Vries, R.G., Snippert, H.J., van de Wetering, M., Barker, N., Stange, D.E., van Es, J.H., Abo, A., Kujala, P., Peters, P.J., and Clevers, H. (2009). Single Lgr5 stem cells build crypt-villus structures in vitro without a mesenchymal niche. *Nature* **459**, 262–265.
- Sato, T., van Es, J.H., Snippert, H.J., Stange, D.E., Vries, R.G., van den Born, M., Barker, N., Shroyer, N.F., van de Wetering, M., and Clevers, H. (2011). Paneth cells constitute the niche for Lgr5 stem cells in intestinal crypts. *Nature* **469**, 415–418.
- Schwitalla, S., Fingerle, A.A., Cammareri, P., Nebelsiek, T., Göktuna, S.I., Ziegler, P.K., Canli, O., Heijmans, J., Huels, D.J., Moreaux, G., et al. (2013). Intestinal tumorigenesis initiated by dedifferentiation and acquisition of stem-cell-like properties. *Cell* **152**, 25–38.
- Soriano, P. (1999). Generalized lacZ expression with the ROSA26 Cre reporter strain. *Nat. Genet.* **21**, 70–71.
- Stange, D.E., Koo, B.-K., Huch, M., Sibbel, G., Basak, O., Lyubimova, A., Kujala, P., Bartfeld, S., Koster, J., Geahlen, J.H., et al. (2013). Differentiated Troy+ chief cells act as reserve stem cells to generate all lineages of the stomach epithelium. *Cell* **155**, 357–368.
- Takeda, N., Jain, R., LeBoeuf, M.R., Wang, Q., Lu, M.M., and Epstein, J.A. (2011). Interconversion between intestinal stem cell populations in distinct niches. *Science* **334**, 1420–1424.
- Tata, P.R., Mou, H., Pardo-Saganta, A., Zhao, R., Prabhu, M., Law, B.M., Vinarsky, V., Cho, J.L., Breton, S., Sahay, A., et al. (2013). Dedifferentiation of committed epithelial cells into stem cells in vivo. *Nature* **503**, 218–223.
- Tian, H., Biehs, B., Warming, S., Leong, K.G., Rangell, L., Klein, O.D., and de Sauvage, F.J. (2011). A reserve stem cell population in small intestine renders Lgr5-positive cells dispensable. *Nature* **478**, 255–259.
- van der Flier, L.G., van Gijn, M.E., Hatzis, P., Kujala, P., Haegebarth, A., Stange, D.E., Begthel, H., van den Born, M., Guryev, V., Oving, I., et al. (2009a). Transcription factor achaete scute-like 2 controls intestinal stem cell fate. *Cell* **136**, 903–912.
- van der Flier, L.G., Haegebarth, A., Stange, D.E., van de Wetering, M., and Clevers, H. (2009b). OLFM4 is a robust marker for stem cells in human intestine and marks a subset of colorectal cancer cells. *Gastroenterology* **137**, 15–17.
- van Es, J.H., Sato, T., van de Wetering, M., Lyubimova, A., Nee, A.N., Gregorieff, A., Sasaki, N., Zeinstra, L., van den Born, M., Korving, J., et al. (2012). Dll1+ secretory progenitor cells revert to stem cells upon crypt damage. *Nat. Cell Biol.* **14**, 1099–1104.
- Vanoaica, L., Darshan, D., Richman, L., Schümann, K., and Kühn, L.C. (2010). Intestinal ferritin H is required for an accurate control of iron absorption. *Cell Metab.* **12**, 273–282.
- Vermeulen, L., Morrissey, E., van der Heijden, M., Nicholson, A.M., Sottoriva, A., Buczacki, S., Kemp, R., Tavaré, S., and Winton, D.J. (2013). Defining stem cell dynamics in models of intestinal tumor initiation. *Science* **342**, 995–998.
- Westphalen, C.B., Asfaha, S., Hayakawa, Y., Takemoto, Y., Lukin, D.J., Nuber, A.H., Brandtner, A., Setlik, W., Remotti, H., Muley, A., et al. (2014). Long-lived intestinal tuft cells serve as colon cancer-initiating cells. *J. Clin. Invest.* **124**, 1283–1295.
- Withers, H.R. (1971). Regeneration of intestinal mucosa after irradiation. *Cancer* **28**, 75–81.
- Zarjou, A., Bolisetty, S., Joseph, R., Traylor, A., Apostolov, E.O., Arosio, P., Balla, J., Verlander, J., Darshan, D., Kuhn, L.C., and Agarwal, A. (2013). Proximal tubule H-ferritin mediates iron trafficking in acute kidney injury. *J. Clin. Invest.* **123**, 4423–4434.